Chinese Chemical Letters 34 (2023) 107204

Contents lists available at ScienceDirect

Chinese Chemical Letters

journal homepage: www.elsevier.com/locate/cclet

Tuning surface sites to boost photocatalytic degradation of phenol and ciprofloxacin

Ran Wen, Long Yang, Sujuan Wu*, Daiqi Zhou, Bin Jiang

College of Materials Science and Engineering, Chongqing University, Chongqing 400044, China

ARTICLE INFO

Article history:
Received 30 November 2021
Revised 25 December 2021
Accepted 6 February 2022
Available online 9 February 2022

Keywords:
BiOBr
CIP and phenol removal
Cu doping
Activity sites

ABSTRACT

There is an urgent demand for tuning the selectivity and activity of the photocatalysts to remove co-existent pollutants simultaneously. Herein, we introduced the surficial activity sites into the bismuth oxybromide (BiOBr), including the Bi/Bi-O defects and hetero Cu atoms, and then the higher photocatalytic activity and selectivity of BiOBr were realized for degradation phenol and ciprofloxacin (CIP). It can be found that the Bi/Bi-O defects played more important role in enhancing the photocatalytic activity for degradation of phenol, while the Cu atoms significantly improved the photocatalytic activity for removing CIP. Moreover, the heterogeneous Cu atoms as the activity sites excited the reaction between phenol and CIP even under dark condition and were beneficial for synchronously removing phenol and CIP. This work provides a feasible way for BiOX photocatalyst to remove co-existent pollutants and may have a practical application.

Since the coronavirus pneumonia epidemic first broke out in 2019, COVID-19 has brought enormous health, economic, environmental and social challenges [1]. Due to the serious infectiousness and variation of the COVID-19, disinfectant water [2,3] and antibiotics were widely used and their usage was far exceeded the expected range. As the main contents of phenolic compounds in disinfectant, phenol is a colorless, moisturizing, highly toxic [4] and difficult to biodegrade [5–7]. When the phenolic compounds entered environment through sewage discharge, it would cause second chemical pollution to threaten human health [8–10]. While for the widely used broad-spectrum antibiotic, ciprofloxacin (CIP), it has been reported that the abuse of CIP can easily induce bacteria variations with drug resistance, thereby forming resistance genes [11,12]. According to a report in September 2018, about 31 mg/L and 14 mg/L of CIP were already detected in the pharmaceutical wastewater produced by the factory and the wastewater produced by urban life, and 2500 and 14 μg/L of CIP were detected in the surface water and groundwater [13–15]. Therefore, how to effectively treat such phenol and CIP coexisted wastewater before they go to global water circles should pay more attention [16].

Recently, several methods, including adsorption, chemical process, condensation, photocatalytic degradation *etc.*, and advanced oxidation, prepolymerization, biodegradation engineering systems, coagulation *etc.* have been reported to remove the phenol and CIP, respectively [17–19]. Among these techniques, semiconductor photocatalytic techniques have been regarded as one of the most effective and "green" methods because they can completely eliminate the organic pollutants in a rapid, cheap and environmentally-friend manner [20,21]. The photocatalysts as the core of the photocatalytic techniques directly determined the photocatalytic activity and selectivity [22]. Bismuth oxybromide (BiOBr) with typical layered structure [23,24], has attracted great attention [25–28] due to the high-efficiency and its visible light responded properties. It does not only have *quasi*-2D [29,30] configuration favoring the formation of layered structure [31] and high interlayer charge separation efficiency, but also has the 2.45 eV band gap and suitable redox potential for degrading pollutants into nontoxic molecules [32–36]. Moreover, Chen *et al.* and Sin *et al.* reported that the BiOBr presents the activity for photocatalytic degradation of antibiotics and phenol, respectively [37,38]. However, efficient removal of two co-existent pollutants is still a great challenge for BiOBr because it mainly depends on its selectivity.

Herein, we proposed the introduction of Cu atoms as hetero activity sites into defective BiOBr to tuning its selectivity and activity. In the individual pollutant system, the existence of intrinsic Bi/Bi-O activity sites [39] enhanced the photocatalytic activity of BiOBr for removing phenol, while the doped Cu atoms were beneficial to removing CIP. In the phenol and CIP co-exist system, both the introduction of Bi/Bi-O and Cu atoms activity sites could realize the efficient removal of phenol and CIP by BiOBr. What is more, the Cu activity sites in BiOBr promoted the reaction between phenol

* Corresponding author.
E-mail address: sujuan.wu@cqu.edu.cn (S. Wu).

https://doi.org/10.1016/j.cclet.2022.02.010
1001-8417/

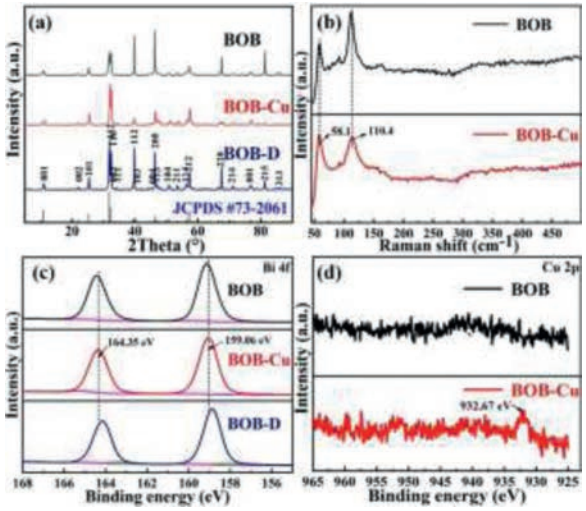

Fig. 1. (a) X-ray diffraction patterns of BOB, BOB-D and BOB-Cu; (b) Raman spectra of BOB and BOB-Cu; (c) XPS spectra of Bi^{3+} in BOB, BOB-D and BOB-Cu and (d) XPS spectra of Cu^{2+} in BOB and BOB-Cu.

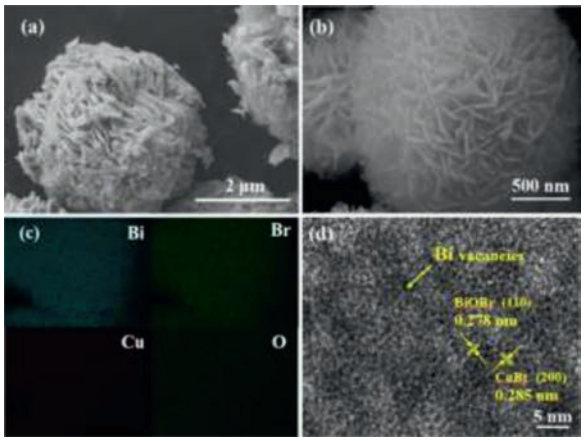

Fig. 2. (a, b) SEM images of BOB-Cu samples, and (c) the elemental mappings of Bi, Br, Cu, O, and (d) HRTEM image of BOB-Cu.

and CIP under dark condition and then presented the highest activity for simultaneously degradation of phenol and CIP. Through the tuning of activity sites, the effective degradation of the co-exist pollutants will be achieved as we expected, which will provide a new way for pollution control in the post-epidemic era.

The BiOBr-Cu photocatalyst was synthesized by the solvothermal method. Specifically, 2 mmol $Bi(NO_3)_3{\cdot}5H_2O$, 2 mmol NaBr, and $CuCl_2$ with a mass ratio of approximately 3 wt% of Cu to Bi were dissolved in 60 mL $C_2H_6O_2$ solution with vigorous stirring for 10 min. Then the mixture was ultrasonically dispersed for 15 min and stirrer at 600 r/min for 2 h in a dark environment. Next, the solution was transferred to a 100 mL Teflon autoclave and kept at 160 °C for 12 h. After cooling to room temperature, the precipitate was collected and washed with deionized water and dried in a vacuum at 80 °C for 12 h to obtain Cu doped BiOBr (BOB-Cu), in which a copper content is 3 wt%. The defective BiOBr (BOB-D) was synthesized *via* a similar synthesis process without $CuCl_2$. The pure BiOBr (BOB) was also obtained through similar synthesis steps, except that the ethylene glycol solvent was instead by pure water. The detailed information of X-ray diffraction (XRD), scanning electron microscope (SEM), energy-dispersive X-ray spectroscopy (EDS), ultraviolet-visible diffuse reflectance spectroscopy (DRS), X-ray photoelectron spectra (XPS), photocurrent (PC) and electrochemical impedance spectroscopy (EIS), and photocatalytic activity characterizations were shown in the supporting information. Their system energy was obtained by the DFT calculations, see Supporting information.

The XRD patterns of the prepared catalysts were shown in Fig. 1a. All of the diffraction peaks can be well indexed with the BiOBr (JCPDS #73–2061), indicating the BiOBr (BOB) has been successfully synthesized. For the Cu doped BiOBr (BOB-Cu), no impurities such as Cu, $CuBr_2$, or CuO were detected even in the samples with different contents of Cu doping (Fig. S1 in Supporting information). Raman spectra were further used to explore the bonding structure of synthesized samples (Fig. 1b). The peaks at 110.5 cm^{-1} and 58 cm^{-1} could be assigned to be A_{1g} internal and A_{1g} external of Bi–Br stretching mode, respectively [40,41]. It is worth noting that the Raman vibration peak located at 110.4 cm^{-1} becomes broadened in BOB-Cu as compared with the pure BOB. It could be attributed to be the interaction between Br and Cu because the Cu–Br stretching mode would introduce a peak at 108 cm^{-1} [42]. This may suggest the formation of the Cu–Br bonds in BOB-Cu.

To investigate the chemical states of BOB with defects and Cu doping, the XPS spectra were further studied. As shown in Fig. 1c, the two individual peaks located at 159.13 eV and 164.46 eV can be associated to Bi $4f_{5/2}$ and Bi $4f_{7/2}$ of Bi^{3+}. These two peaks slightly shift to low binding energy, and are accompanied by the emergency of new couple peaks at 158.84 eV and 164.16 eV in the BOB-D, indicating the formation of low valence $Bi^{(3-x)+}$ due to the existence of defects. According to our previous work, the existence of Bi and Bi-O defects in bismuth based photocatalysts would result in the slightly shift for lower binding energy and then we proposed the formation of Bi/Bi-O defects in defective BiOBr (BOB-D) [43,44]. However, barely shift were observed in BOB-Cu. It may demonstrate that the hetero Cu atoms would stay at the position of Bi/Bi-O defects and the Cu doped into the BOB-D. More vivid evidence can be found in the XPS spectra of Cu 2p (Fig. 1d). Compare with BOB-D, a small peak that appears at 932.67 eV can be assigned to Cu $2p_{3/2}$ of Cu^{2+}, which is lower than the standard binding energy of Cu $2p_{3/2}$ of Cu^{2+} (933.3 eV) [45]. It was thus deduced that Cu atoms have been successfully introduced into the BOB.

The morphologies of as-synthesized samples were further evaluated by scanning electron microscopy (SEM), as shown in Figs. 2a and b and Fig. S2 (Supporting information). The BOB, BOB-D and BOB-Cu possess a similar spherical structure, but detailed results suggest that these spherical structure was consisted by the nanosheets with the thickness of about 20 nm. This morphology agreed well with Wei *et al.* [46] and Hua *et al.* [47] report and is a benefit for promoting the photocatalytic activity. No matter introducing of intrinsic defects or Cu atoms doping, the morphology of the BiOBr maintained the same, demonstrating that the further improvement on the photocatalytic activity would not be attributed to be the morphology. The 3% Cu atoms enabled the observation of Cu in BOB-Cu by EDS mapping was not obvious, but it still can be deduced from Fig. 2c that the distribution of the Cu atoms is not in cluster. Fig. 2d showed the microstructure of BOB-Cu, in which the lattice fringes of 0.278 nm and 0.285 nm are well matched with the (110) planes of BiOBr and (200) planes of CuBr, respectively. In addition, the Bi vacancies can be observed in the disordered area. This results not only verified the existence of Bi/Bi-O defects, but also demonstrated the hetero Cu atoms tent to bonding with unmatched Br atoms.

To further verify the stability of Cu atoms in defective BOB, we built atomic structure models of BOB, BOB-D, BOB-Cu (Fig. S3 in Supporting information) based on the previously reported atomic structure of BOB [48,49] and calculated their system energy (Table S1 in Supporting information). Considering the uncertainty of the position of Cu atoms, we first proposed that the Cu atoms as

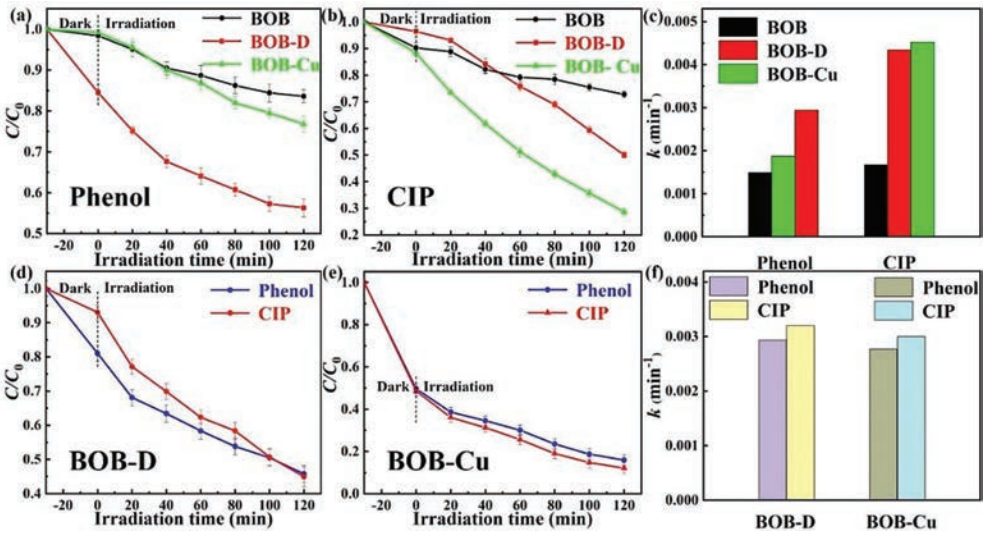

Fig. 3. (a) Photocatalytic degradation of phenol and (b) CIP by different catalysts under visible light irradiation and (c) the calcaultated photocatalytic degradation rate of different photocatalysts. Photocatalytic degradation of phenol and CIP mixed solution by (d) BOB-D, (e) BOB-Cu photocatalyst under visible light irradiation and (f) the calculated photocatalytic degradation rate of different photocatalysts.

exert atoms stayed on the Bi vacancies and interacted with the Br atoms to maintain the stability of the BiOBr, as illustrated in Fig. S3c. Then we proposed that Cu atoms located above the Bi vacancies and no interaction with the neighboring atoms, as shown in Fig. S4 (Supporting information). According to our calculation, the BiOBr with Cu atoms as exert atoms stay on the Bi vacancies showed the lowest energy, in line with the HRTEM observation of CuBr in BOB-Cu. It was thus deduced that the Cu doping is much stable in defective BOB and these hetero atoms may instead the intrinsic vacancies and further affect the photocatalytic activity. The photocatalytic performance of the samples was evaluated by photocatalytic degradation of phenol and ciprofloxacin (CIP) solution under visible light. As shown in Fig. 3a, the removal of phenol was only around ~16.5% by pure BOB and ~23.3% by BOB-Cu after 2 h, but it became to be ~43.7% by BOB-D. The BOB-D presented much higher adsorption and photocatalytic activity for photocatalytic degradation of phenol. In contrast, the BOB-Cu showed the highest photocatalytic activity for degradation of CIP. It is around 1.65 times and 1.43 times higher than that of BOB and BOB-D (Fig. 3b). Based on the calculated degradation rate in Fig. 3c, the photocatalytic activity of BOB was significantly enhanced by introducing the activity sites. The intrinsic Bi/Bi-O defects play more important role in improvement the photocatalytic activity for phenol degradation, while the hetero Cu atoms have a major effect on the photocatalytic degradation of CIP.

We further carried out the photocatalytic degradation experiment of the mixed solution of phenol and CIP. The photocatalytic activity of BOB-D (Fig. 3d) and BOB-Cu (Fig. 3e) were significantly increased for degradation co-existent phenol and CIP as compared with the previously separated one. For BOB-D, it was interesting to find that the final degradation rate for phenol and CIP were achieved to be the same, although the adsorption of 7% in CIP and 19% in phenol at the beginning dark adsorption stage. While for BOB-Cu, the degradation rate of phenol and CIP reached to almost 84.2% and 88%, but it was noticed that the decrement of phenol and CIP in the dark adsorption stage is equivalent. It thus can be deduced that the reaction between phenol and CIP could be promoted by the BOB-Cu catalysts. The existence of Cu atoms leads to higher catalytic activity for the reaction between phenol and CIP, and further improved the photocatalytic activity of the mixed solution (Fig. 3f). This further verified the photocatalytic selectivity of the BiOBr was tuned by introduction of Cu atoms as activity sites.

The ultraviolet-visible diffuse reflectance spectra of samples were shown in Fig. 4a. It was found that all the samples had absorption in the visible region. The absorption range was extended from 425 nm for BOB to be 450 nm for BOB-D and 490 nm for BOB-Cu, and the corresponded band gap was estimated to be 2.44 eV 2.35 eV and 2.17 eV, respectively (Fig. 4a (insert)) [50]. The band gap of BOB had been slightly narrowed after introducing defect and following Cu doping. The photocurrent response of samples under visible light were shown in Fig. 4b. It showed that all these samples possess a good response of generating photo-induced carries after activating by the visible light. The photocurrent density was significantly enhanced in BOB-D and BOB-Cu, suggesting that the introduction of these activity sites was a benefit for the separation of the photo-excited electron-hole pairs. Then, electrochemical impedance spectroscopy (EIS) was used to evaluate the charge separation efficiency (Fig. 4c). The charge-transfer resistance can be deduced from the diameter of the high-frequency semicircle in the Nyquist diagram. It is widely accepted that the smaller diameter semicircles indicate lower charge-carrier transfer resistance and faster interfacial charge-carrier migration [51]. So it was further verified that the introduction of the activity sites can decrease the charge-carrier transfer resistance and be beneficial for the charge transfer.

Furthermore, Mott-Schottky experiment was conducted to evaluate the band positions of the samples (Fig. 4d). The slope of the linear $1/C^2$ potential curves was negative, indicating that BiOBr is a p-type semiconductor characteristic and the doping does not affect the intrinsically p-type behavior. The flat-band potential versus RHE was then calculated to be BOB (+1.50 eV), BOB-D (+1.43 eV) and BOB-Cu (+1.36 eV), and the valence band (VB) potential of the samples was thus estimated to be 1.26 eV, 1.19 eV, and 1.12 eV, respectively. Therefore, the conduction band were deduced to be −1.18 eV, −1.16 eV, and −1.05 eV. It was worth noting that the photo-induced holes on VB of BOB-D and BOB-Cu cannot oxidize H_2O to $^{\bullet}OH$ radical because the standard redox potential of $H_2O/^{\bullet}OH$ (+2.38 V, NHE pH 0) was more positive than the valence band maximum of BOB-D (+1.19 eV) and BOB-Cu (+1.12 eV) [52]. However, the photo-induced electrons on CB of BOB-D and BOB-Cu can reduce O_2 to $^{\bullet}O_2^-$ radicals because the potential of conduction band minimum of BOB-D (−1.16 eV) and BOB-Cu (−1.05 eV) was more negative than the standard redox potential of $O_2/^{\bullet}O_2^-$ (−0.326 V, NHE pH 0) [52,53]. Herein,

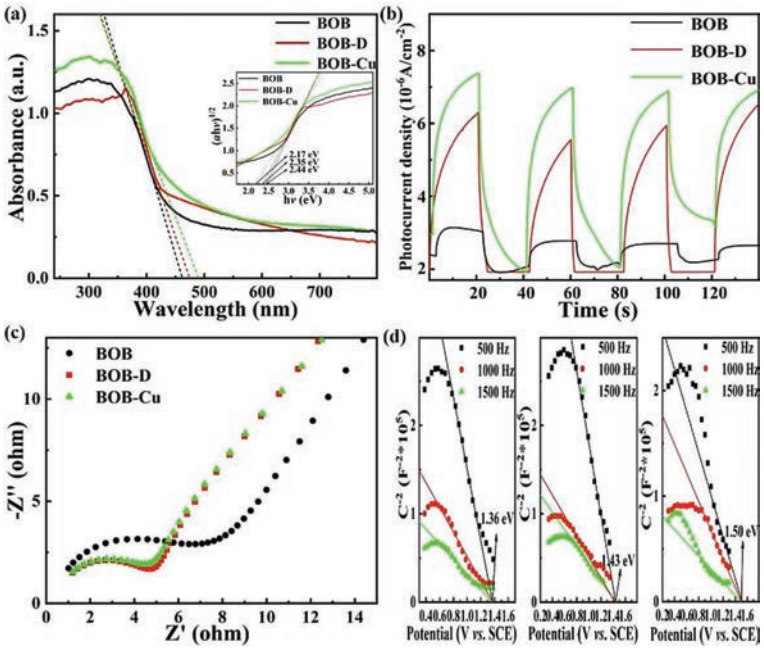

Fig. 4. (a) The UV-vis spectrum and its band gap diagram (see insert illustration), (b) the spectrum of photocurrent and (c) EIS of different catalysts, and (d) Mott-Schottky plots of BOB, BOB-D, BOB-Cu.

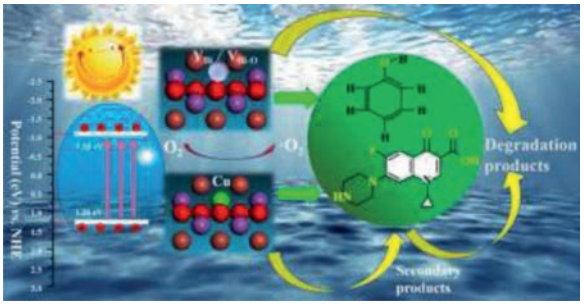

Fig. 5. The possible mechanism for phenol and CIP degradation over the BOB-D and BOB-Cu catalyst under visible light irradiation.

the $^{\bullet}O_2^-$ radicals would be the main active substances during the photocatalysis.

Accordingly, the photocatalytic degradation mechanism of phenol and CIP by BOB-D and BOB-Cu photocatalysts was illustrated in Fig. 5. Surface defects engineering had become an effective way to improve the performance of photocatalysts [54–56]. By introducing Bi/Bi-O defects and doped Cu atoms, the light absorption range was extended and meanwhile the charge recombination rate was decreased, result in the enhancement of the photocatalytic activity. Nonetheless, the Bi/Bi-O defects as activity sites selectively promoted degradation of phenol, while the hetero Cu atoms tuned to improve the photocatalytic activity for CIP degradation. Both of these photocatalytic reactions were performed *via* $^{\bullet}O_2^-$ induced reduction. Herein, the Bi/BiO vacancies offered the position for holding the hetero Cu atoms and responded for tuning the charge separation and selectivity of BOB. The Cu atoms as activity sites not only take the advantage of charge separation in photocatalysis, but also benefit for the reaction between CIP and phenol without irradiation. Therefore, the higher activity and selectivity of BOB photocalytst for the degradation of mixed solution was achieved by tuning the activity sites.

In summary, we introduced Bi/BiO defects and Cu atoms in BiOBr by solvothermal method. Due to the existence of surficial Bi/Bi-O and Cu atoms defects, the BiOBr photocatalysts present higher photocatalytic activity and selectivity in degradation of phenol and CIP. These defects not only enable the extension of the photo-absorption range and decrease the recombination of the photo-excited charges, but also they could act as the activity sites to improve the photocatalytic selectivity of BiOBr by tuning the adsorption and degradation of different pollutant. More important, these activity sites accelerate the reaction between two pollutant under dark condition and further promote the photocatalytic reaction of the mixed solution and photocalysts. Therefore, this work develops a new strategy for removing co-existent pollutants of phenol and CIP by tuning the activity sites of BiOBr, and also provides some new insights for realizing the co-catalyst reaction *via* synergistic effect.

Declaration of competing interest

The authors declare no competing financial interest.

Acknowledgments

This research was financially supported by the Chongqing Research Program of Basic Research and Frontier Technology (No. cstc2018jcyjAX0408). S. Wu gratefully acknowledges support from Yuqi Zhang and Wen Zeng.

Supplementary materials

Supplementary material associated with this article can be found, in the online version, at doi:10.1016/j.cclet.2022.02.010.

References

[1] I. Chakraborty, P. Maity, Sci. Total Environ. 728 (2020) 138882.
[2] K.S. Khoo, L.Y. Ho, H.R. Lim, et al., J. Hazard. Mater. 417 (2021) 126108.
[3] J. Schwartz, C.C. King, M.Y. Yen, Clin. Infect. Dis. 71 (2020) 858–860.
[4] Y.M. Dong, G.L. Wang, P.P. Jiang, et al., Chin. Chem. Lett. 22 (2011) 209–212.
[5] B. Pare, P. Singh, S.B. Jonnalgadda, Indian J. Chem. SEC A 48 (2009) 1364–1369.
[6] P. Raizada, J. Kumari, P. Shandilya, P. Singh, Desalin. Water Treat. 79 (2017) 204–213.
[7] H. Wang, Y. Wu, M. Feng, et al., Water Res. 144 (2018) 215–225.

[8] M.V.A. Corpuz, A. Buonerba, G. Vigliotta, et al., Sci. Total Environ. 745 (2020) 140910.
[9] K. Fan, C. Yu, S. Cheng, et al., Surf. Interfaces 26 (2021) 101335.
[10] M. Zhang, J. He, Y. Chen, et al., Chin. Chem. Lett. 31 (2020) 2721–2724.
[11] K. Hu, R. Li, C. Ye, et al., J. Cleaner Prod. 253 (2020) 120055.
[12] X. Xu, X. Ding, X. Yang, et al., J. Hazard. Mater. 364 (2019) 691–699.
[13] P. Kovalakova, L. Cizmas, T.J. McDonald, et al., Chemosphere 251 (2020) 126351.
[14] S. Li, T. Huang, P. Du, et al., Water Res. 185 (2020) 116286.
[15] S. Li, W. Shi, H. Li, et al., Sci. Total Environ. 636 (2018) 1009–1019.
[16] W. Ali, H. Zhang, Z. Wang, et al., J. Hazard. Mater. 414 (2021) 125439.
[17] P. Singh, P.R. Sonu, et al., J. Saudi Chem. Soc. 23 (2019) 586–599.
[18] T.Y. Tan, Z.T. Zeng, G.M. Zeng, et al., Sep. Purif. Technol. 235 (2020) 116167.
[19] M. Yu, H. Liang, R. Zhan, et al., Chin. Chem. Lett. 32 (2021) 2155–2158.
[20] H. Tong, S. Ouyang, Y. Bi, et al., Adv. Mater. 24 (2012) 229–251.
[21] S. Wu, Z. Xu, J. Zhang, M. Zhu, Sol. RRL 5 (2021) 2100668.
[22] J. Di, C. Chen, C. Zhu, et al., Adv. Energy Mater. 11 (2021) 2102389.
[23] W.L. Huang, Q. Zhu, Comput. Mater. Sci. 43 (2008) 1101–1108.
[24] K.L. Zhang, C.M. Liu, F.Q. Huang, et al., Appl. Catal. B: Environ. 68 (2006) 125–129.
[25] N.T. Hahn, S. Hoang, J.L. Self, C.B. Mullins, ACS Nano 6 (2012) 7712–7722.
[26] J. Jiang, K. Zhao, X. Xiao, L. Zhang, J. Am. Chem. Soc. 134 (2012) 4473–4476.
[27] X. Xiao, W.D. Zhang, RSC Adv. 1 (2011) 1099–1105.
[28] L. Ye, L. Zan, L. Tian, et al., Chem. Commun. 47 (2011) 6951–6953.
[29] S. Wu, J. Sun, Q. Li, et al., ACS Appl. Mater. Interfaces 12 (2020) 20067–20074.
[30] W. Zhong, B. Xiao, Z. Lin, et al., Adv. Mater. 33 (2021) 2007894.
[31] S. Wu, J. Sun, S.Z. Yang, et al., Inorg. Chem. 57 (2018) 8988–8993.
[32] Y. Bu, H. Li, W. Yu, et al., Environ. Sci. Technol. 55 (2021) 2110–2120.
[33] D. Liu, D. Chen, N. Li, et al., Angew. Chem. Int. Ed. 59 (2020) 4519–4524.
[34] X. Wang, G. Xu, Y. Tu, et al., Chem. Eng. J. 411 (2021) 128456.
[35] H. Yu, H. Huang, K. Xu, et al., ACS Sustainable Chem. Eng. 5 (2017) 10499–10508.
[36] M. Zhang, Y. Qi, Z. Zhang, Polymers (Basel) 11 (2019) 111718.
[37] J.C. Sin, C.A. Lim, S.M. Lam, et al., Mater. Lett. 248 (2019) 20–23.
[38] X. Zhang, R. Li, M. Jia, et al., Chem. Eng. J. 274 (2015) 290–297.
[39] S. Wu, W. Sun, J. Sun, et al., Chem. Mater. 30 (2018) 5128–5136.
[40] A. Phuruangrat, S. Thongtem, T. Thongtem, J. Electron. Mater. 48 (2019) 8031–8038.
[41] D. Zhang, J. Li, Q. Wang, Q. Wu, J. Mater. Chem. A 1 (2013) 8622–8629.
[42] M. Bochalya, P.K. Kanaujia, G.V. Prakash, S. Kumar, J. Solid State Chem. 273 (2019) 219–225.
[43] L. Zhu, Y. Wu, S. Wu, et al., ACS Appl. Mater. Interfaces 13 (2021) 9216–9223.
[44] J. Di, C. Chen, S.Z. Yang, et al., Nat. Commun. 10 (2019) 1–7.
[45] Z. Li, X. Huang, L. Lin, et al., Chem. Eng. J. 419 (2021) 129488.
[46] Z.D. Wei, R. Wang, Chin. Chem. Lett. 27 (2016) 769–772.
[47] C. Hua, X. Dong, Y. Wang, et al., J. Mater. Sci. 54 (2019) 9397–9413.
[48] J. Chen, M. Guan, W. Cai, et al., Phys. Chem. Chem. Phys. 16 (2014) 20909–20914.
[49] C.Y. Wang, Q. Zeng, G. Zhu, Chemosphere 268 (2021) 128854.
[50] C. Zhao, Y. Li, H. Chu, et al., J. Hazard. Mater. 419 (2021) 126466.
[51] H. Li, S. Wu, Z.D. Hood, et al., Appl. Surf. Sci. 513 (2020) 145723.
[52] Y. Nosaka, A.Y. Nosaka, Chem. Rev. 117 (2017) 11302–11336.
[53] X.A. Dong, W. Zhang, Y. Sun, et al., J. Catal. 357 (2018) 41–50.
[54] Z. Lin, B. Xiao, Z. Wang, et al., Adv. Funct. Mater. 31 (2021) 2102321.
[55] Z. Wang, B. Xiao, Z. Lin, et al., Angew. Chem. Int. Ed. 60 (2021) 23388–23393.
[56] W. Zhong, Z. Wang, N. Gao, et al., Angew. Chem. Int. Ed. 59 (2020) 22743–22748.